THE JOURNAL OF PHYSICAL CHEMISTRY C

Article

pubs.acs.org/JPCC

Dynamics of Pyramidal SiH_3^- Ions in $ASiH_3$ (A = K and Rb) Investigated with Quasielastic Neutron Scattering

Carin Österberg,[†] Henrik Fahlquist,[‡] Ulrich Häussermann,[‡] Craig M. Brown,[§] Terrence J. Udovic,[§] and Maths Karlsson*[,†]

[†]Department of Physics, Chalmers University of Technology, SE-412 96 Göteborg, Sweden

[‡]Department of Materials and Environmental Chemistry, Stockholm University, SE-10691 Stockholm, Sweden

[§]NIST Center for Neutron Research, National Institute of Standards and Technology, 100 Bureau Drive, Gaithersburg, Maryland 20899-6102, United States

Supporting Information

ABSTRACT: The two alkali silanides $ASiH_3$ (A = K and Rb) were investigated by means of quasielastic neutron scattering, both below and above the order−disorder phase transition occurring at around 275−300 K. Measurements upon heating show that there is a large change in the dynamics on going through the phase transition, whereas measurements upon cooling reveal a strong hysteresis due to undercooling of the disordered phase. The results show that the dynamics is associated with rotational diffusion of SiH_3^- anions, adequately modeled by H-jumps among 24 different jump locations radially distributed around the Si atom. The average relaxation time between successive jumps is of the order of subpicoseconds and exhibits a weak temperature dependence with a small difference in activation energy between the two materials, 39(1) meV for $KSiH_3$ and 33(1) meV for $RbSiH_3$. The pronounced SiH_3^- dynamics explains the high entropy observed in the disordered phase resulting in the low entropy variation for hydrogen absorption/desorption and hence the origin of these materials' favorable hydrogen storage properties.

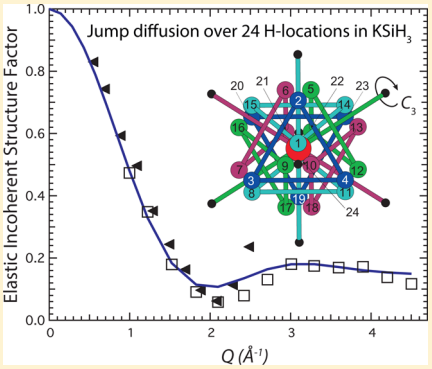

1. INTRODUCTION

Currently, there is a large effort devoted to the development of technologies that use hydrogen as an energy source. A specific challenge is to design a hydrogen storage material that is safe, economic, and efficient.[1,2] Recently, it has been shown that the hydrogenation of the ASi (A = K, Rb and Cs) Zintl phases gives alkali metal silyl hydrides $ASiH_3$ (A = K, Rb and Cs), which are able to respectively store up to 4.3, 2.6, and 1.85 wt % of H_2 reversibly with a good *P-T* window; a 0.1 MPa hydrogen equilibrium pressure can be obtained at around 414 K, which is compatible with proton exchange membrane (PEM) fuel-cell applications.[3,4] This adds to the expanding list of promising complex hydrides for hydrogen storage applications, such as amides $M(NH_2)_x$, imides $M(NH)_{x/2}$,[5,6] borohydrides $M(BH_4)_x$,[7−12] and alanates $M(AlH_4)_x$ and $M_x(AlH_6)_y$,[13,14] which are already well investigated in the literature, and also the recently investigated amido-boranes $M(NH_2BH_3)_x$,[15] ammonium-closo-borane $(NH_4)_2B_{12}H_{12}$,[16] and hydrazinido-boranes $M(N_2H_3BH_3)_x$.[17]

At room temperature, the crystal structure of $ASiH_3$ corresponds to an average cubic NaCl-type arrangement of alkali metal and Si atoms, meaning that pyramidal anions SiH_3^- are distributed in random orientations in the crystal structure (α-$ASiH_3$).[18,19] Specifically, recent structural analysis based on neutron diffraction data on the deuterated equivalents α-$ASiD_3$ (A = K, Rb and Cs), has established a structure of D atoms distributed on a weakly occupied (12%) Wyckoff site 96*k* (space group $Fm\bar{3}m$), for all three materials.[4] This means that the distribution of the D atoms may be represented by a quasi-spherical environment with 24 D atom positions surrounding one Si atom.[3,4] This simple model provides a very reasonable crystallographic description of the disorder in which pyramidal SiH_3^- ions are randomly aligned along one of the four body diagonals (i.e., the C_3 axes) of a silicon-centered cube.,[3,4,19] cf. Figure 1. In addition, each body diagonal direction allows for an "up" and "down" alignment. Thus, the average crystallographic structure of α-$ASiH_3$ is based on eight (random) orientations for each SiH_3^- ion (Figure 1). At temperatures below 200 K, $ASiH_3$ compounds exist as hydrogen-ordered β modifications.[3,4,20,21] β-$KSiH_3$ crystallizes in the orthorhombic *Pnma* space group, whereas β-$RbSiH_3$ and β-$CsSiH_3$ crystallize in the monoclinic $P2_1/m$ space group.[4] On the basis of differential thermal analysis of ASiH3, a reversible phase transition was observed between the high-temperature α-phase and low-temperature β-phase on cooling (at around 240 K) and the reverse (β to α) on heating (at around 300 K and 280 K for A = K and Rb, respectively), thus indicating some hysteresis in these materials.[4]

Received: January 12, 2016
Revised: March 2, 2016
Published: March 4, 2016

DOI: 10.1021/acs.jpcc.6b00363
J. Phys. Chem. C 2016, 120, 6369−6376

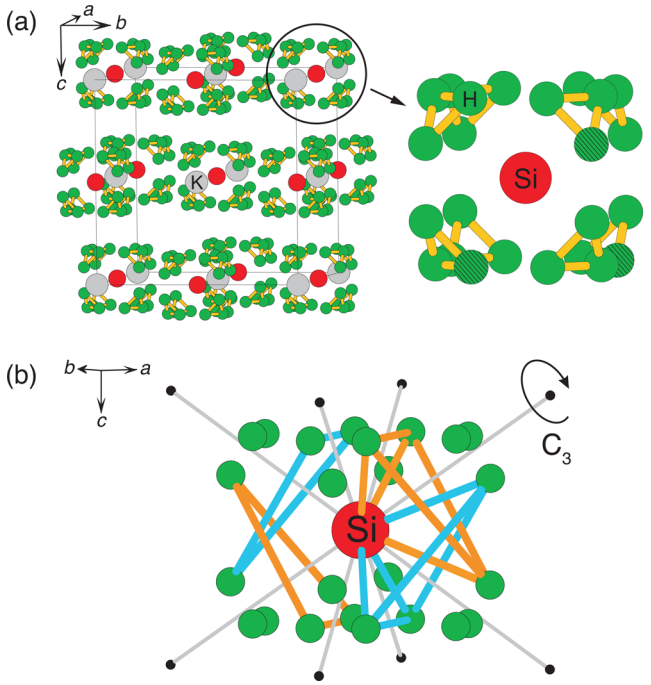

Figure 1. (a) Structural model for disordered α-$KSiD_3$ representing a cubic NaCl-type arrangement of K and Si atoms (space group $Fm\bar{3}m$). H atoms distribute according to a 96*k* Wyckoff site (occupancy 12%). This yields a quasi-spherical environment of 24 H atom positions around each Si atom. The location of the three H atoms belonging to a single SiH_3^- ion are distinguished by dashed patterning. (b) The 24 H atom environment as a consequence of aligning pyramidal SiH_3^- ions (with respect to their C_3 axis) randomly along the four body diagonals of the cubic unit cell (gray lines). This yields eight possible orientations of which four (two "up" and "down" alignments) are emphasized in the figure (light blue and orange bonds).

The favorable thermodynamic characteristics of the hydrogen sorption/desorption process of ASi/α-$ASiH_3$, is due to an unusually low entropy variation, which in turn has been attributed to the disorder in α-$ASiH_3$. Recent infrared and Raman spectroscopy investigations indicated that the disordered nature of α-$ASiH_3$ relates to quasi-freely rotating SiH_3^- moieties, with C_{3v} symmetry and which are confined to the octahedral cavity of six A^+ cations in the NaCl-type structure.[21] Particularly strong evidence of pronounced dynamics comes from the slightly but distinctly different structure and vibrational properties of SiH_3^- anions in low-temperature β-$ASiH_3$ and room-temperature α-$ASiH_3$.[21] In fact, the vibrational properties of SiH_3^- in α-$ASiH_3$ relate well to those of silyl anions in polar aprotic solvents. Its structural properties correspond to that of a slightly compressed gas-phase species (Si−H bond length =1.52 Å; H−Si−H angle 92.2°). However, the dynamics of SiH_3^- anions in α-$ASiH_3$ have never been directly investigated, and, in particular, details such as the time-scale, activation energy, and exact spatial geometry of the dynamics, and its relation to the materials' hydrogen-storage properties, have not yet been established.

For this reason, we investigate here the dynamical behavior of SiH_3^- anions in alkali silanides. The investigations are carried out by means of quasielastic neutron scattering (QENS), which is a powerful tool as it gives access to the relevant time- and length-scales on which the atomic-scale dynamics of hydrogen occur. In addition, the very large incoherent neutron scattering cross section of hydrogen compared to all other nuclei in alkali silanides provides a good signal, predominantly related to hydrogen dynamics, in the experiment.[22] The aim of the study is to directly observe and investigate in detail the dynamical behavior of SiH_3^- in α-$ASiH_3$, as well as to elucidate the dependence on the type of alkali ion, compare with the well-studied dynamics of borohydrides,[9,10,23−25] and provide insight into the low entropy variation upon hydrogen absorption/desorption.

We show that there is a large change in the dynamics of SiH_3^- in $KSiH_3$ and $RbSiH_3$ on going through the β−α phase transition. A comprehensive analysis of the QENS data suggests that the SiH_3^- dynamics undergo reorientations akin to rotational diffusion, modeled by jumps between 24 different H sites distributed around the Si atom. This is in agreement with the structure shown in Figure 1b. The relaxation time between jumps are of the order subpicoseconds, with activation energies of around 39(1) meV ($KSiH_3$) and 33(1) meV ($RbSiH_3$), respectively. The pronounced SiH_3^- dynamics explains the high entropy observed in the disordered phase resulting in the low entropy variation for hydrogen absorption/desorption and hence the origin of these materials' favorable hydrogen storage properties. Although $CsSiH_3$ is known, we restricted our investigation to $KSiH_3$ and $RbSiH_3$.

2. EXPERIMENTAL SECTION

2.1. Sample Preparation. Synthesis and sample preparation were performed in an Ar filled glovebox where KSi and RbSi were prepared from stoichiometric amounts of metal ingots, K (Aldrich,[26] 99.9%) and Rb (Aldrich, 99.9%), respectively, and Si powder (Chempur, crystalline powder, 99.999%). The metal was placed inside a stainless steel tube and Si powder was pressed into pellets that were placed on top of the metal. The tube was turned into an ampule and closed by arc welding. The ampules were heated inside a box furnace at a rate of 5 K/min to 873 K, held for 30 h and then cooled to room temperature at a rate of 5 K/min. To prepare $KSiH_3$ and $RbSiH_3$, pellets of KSi and RbSi were heated to 423 and 373 K, respectively, in a corundum crucible in a stainless steel autoclave under a pressure of 50 bar of hydrogen for 24 h (H_2 AGA 99.99999%). Powder X-ray diffraction measurements confirmed phase purity for both samples.

2.2. QENS Experiments. The QENS experiments were performed at the time-of-flight disk chopper spectrometer (DCS)[27] at the NIST Center for Neutron Research, Gaithersburg (USA). All sample preparation for the neutron scattering experiments were performed inside a He-atmosphere glovebox. The materials were carefully ground into fine powders (approximately 2.5 g of $KSiH_3$ and 2 g of $RbSiH_3$) and thinly distributed inside aluminum foil packets subsequently rolled into 100 mm long annuli with diameters of 17.5 mm. Indium wire sealed aluminum cans were used as sample holders and cadmium beam masks were used on the top and bottom of the cans. A closed-cycle refrigerator was used to reach the desired temperatures.

Measurements were performed using two neutron wavelengths, 2.5 and 4.8 Å. For 2.5 Å neutrons, the energy resolution and accessible *Q*-range of the spectrometer were 745 μeV full width at half-maximum and 0.98−4.48 $Å^{-1}$, respectively. For 4.8 Å neutrons, the respective values were 110 μeV and 0.52−2.46 $Å^{-1}$. The typical measuring time was between 2 and 4 h. For $KSiH_3$, spectra were measured at 310, 300, 293, 285, 275, 273, 270, 268, 265, 260, 255, 250, and 50 K (in that order, i.e., upon cooling), using both neutron

DOI: 10.1021/acs.jpcc.6b00363
J. Phys. Chem. C 2016, 120, 6369−6376

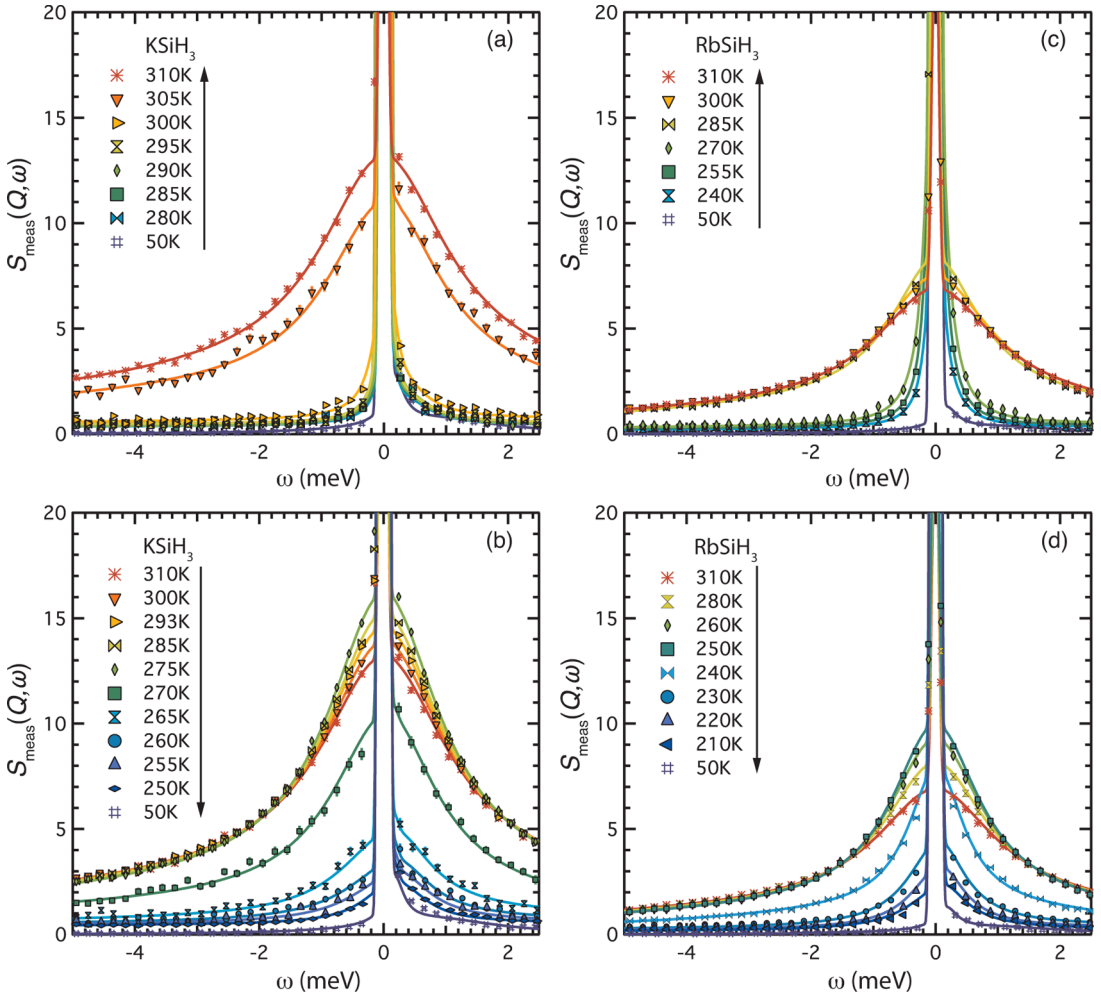

Figure 2. Temperature dependence of the QENS spectra, $S_{meas}(Q, \omega)$, for $KSiH_3$ (a,b) and for $RbSiH_3$ (c,d) at $Q = 1.9$ Å^{-1}, measured with 4.8 Å neutrons. The solid lines are total fits to the data (symbols) according to eq 5.

wavelengths. Spectra were also measured upon heating, at 275, 280, 285, 290, 295, 300, 305, and 310 K, with 4.8 Å neutrons. For $RbSiH_3$, spectra were measured at 310, 280, 260, 250, 240, 230, 220, 210, and 50 K (upon cooling), using both neutron wavelengths. Spectra were also measured upon heating, at 240, 255, 270, 285, 300, and 310 K, with 4.8 Å neutrons. Measurements of an empty cell and a vanadium standard, as well as a dark count measurement, were used for the background correction. The spectra measured at 50 K were used as resolution functions in the data analysis. The QENS spectra were reduced and analyzed using the DAVE[28] software.

3. QENS ON ALKALI SILANIDES

The obtained quantity in most QENS experiments is the dynamical structure factor, $S(Q, \omega)$, which can be separated into one coherent and one incoherent component. The coherent part gives information about interference effects in materials, thus it provides information about the behavior of atoms in relation to each other, whereas the incoherent part relates to scattering from individual atoms. However, in studies of hydrogen dynamics, the very large incoherent neutron scattering cross section of hydrogen, at least an order of magnitude larger than all other elements, and relatively small coherent scattering cross section, enables one to observe hydrogens essentially free from constructive interference. Information about hydrogen self-dynamics can therefore be obtained, whereas the correlation between the dynamical behavior of an ensemble of hydrogens can be neglected. It follows that the total dynamical structure factor can, in our case, be well approximated with the incoherent dynamical structure factor, i.e., $S(Q, \omega) \approx S_{inc}(Q, \omega)$.

In practice, the measured structure factor is a convolution of $S_{inc}(Q, \omega)$ and the resolution function of the instrument, $R(Q, \omega)$, i.e.

$$S_{meas}(Q, \omega) = S_{inc}(Q, \omega) \otimes R(Q, \omega) \quad (1)$$

In the case of quasielastic scattering, $S_{inc}(Q, \omega)$ may be expressed as

$$S_{inc}(Q, \omega) = A_0(Q)\delta(\omega) + \sum_i A_i(Q)L_i(Q, \omega) \quad (2)$$

where the $L_i(Q, \omega)$s are Lorentzian functions of the form

$$L_i(Q, \omega) = \frac{2}{\pi} \frac{\Gamma_i(Q)}{(2\hbar\omega)^2 + \Gamma_i(Q)^2} \quad (3)$$

in which $\hbar\omega$ is the neutron energy transfer and $\Gamma_i(Q)$ the ith Lorentzian's full width at half-maximum. $\Gamma_i(Q)$ relates to a characteristic relaxation, also known as correlation, time, τ_i, according to

DOI: 10.1021/acs.jpcc.6b00363
J. Phys. Chem. C 2016, 120, 6369−6376

$$\tau_i = \frac{2\hbar}{\Gamma_i} \quad (4)$$

The Lorentzian functions thus represent the quasielastic scattering, which appears as a broadening of the elastic line and contains information about both the time-scale and Q-dependence of the observed dynamics.

4. RESULTS AND DISCUSSION

4.1. General Observations of the QENS Spectra. Figure 2 displays the dynamical structure factor, $S_{meas}(Q, \omega)$, as measured upon heating (a,c) and cooling (b,d), both below and above the order−disorder phase transition temperature, for both materials. First we discuss the spectra in a qualitative way, before deducing the time-scale, activation energy, and spatial geometry of the dynamics in more detail. For clarity, only the spectra as measured at Q = 1.9 Å^{-1}, at the higher-resolution (4.8 Å neutrons) are shown. It is immediately apparent that both materials exhibit a strong quasielastic component at the higher temperatures. More specifically, the spectra generally show a noticeable, nonlinear, change in the relative elastic and quasielastic scattering intensities depending on temperature. Considering first the spectra measured upon heating from 50 K [Figure 2(a,c)], we observe essentially no change of the spectra up to about 300 K for $KSiH_3$ and 285 K for $RbSiH_3$, where there is an abrupt change of the spectra with the onset of strong quasielastic scattering. This is in good agreement with differential thermal analysis measurements,[4] which show that the $\beta-\alpha$ phase transition occurs at around 305 K for $KSiH_3$ and 280 K for $RbSiH_3$. Upon further increase of the temperature, the spectra change only slightly.

Considering next the spectra measured upon cooling from 310 K [Figure 2(b,d)], we observe only small changes over the temperature range from 310 to 275 K for $KSiH_3$ and from 310 to 250 K for $RbSiH_3$. Upon further cooling, across the disorder−order phase transition, the spectra do not exhibit that abrupt change as upon heating because on cooling the α-phase is undercooled and the degree of disorder remains relatively high. At 250 K for $KSiH_3$ and 210 K for $RbSiH_3$, the quasielastic scattering is essentially gone, suggesting that there is a large change in the dynamics of these systems on going through the $\alpha-\beta$ transition on the time-scale probed by DCS. The weak, yet clearly observable, quasielastic scattering in the low-temperature β-$ASiH_3$ phase most likely originates from small domains of the dynamically disordered α-$ASiH_3$ phase present in the former. However, the possible presence and nature of slower low-temperature dynamics cannot be excluded and will therefore be subject for a future investigation. A comparison with previous results obtained from nuclear magnetic resonance studies of $ASiH_3$ (A = K, Rb, and Cs) revealed the presence of H dynamics all the way down to 173 K.[19] Thus, the temperature at which the spectra change abruptly is different depending on whether the samples are being cooled or heated, suggesting that the structural phase transition is highly hysteretic. This hysteretic behavior is in general agreement with differential thermal analysis measurements.[4]

Our more detailed analysis of the QENS spectra focuses on the high-temperature α-phase. The QENS spectra were fit with a function comprised of one elastic component together with two Lorentzian functions. It should be noted that initial attempts to fit the QENS spectra utilized one Lorentzian function. It was only when it was apparent that one Lorentzian fits inadequately to the spectra, that a second Lorentzian was added. The second Lorentzian, however, is so broad (a $\Gamma(Q)$ of 7 meV at low Qs up to 50 meV at high Qs) that we only consider it as a background originating from mainly vibrational modes (i.e., inelastic scattering) occurring at energy transfers larger than zero but overlapping with the quasielastic region. The resulting line width of the narrower Lorentzian, $\Gamma_{1'}(Q)$, is shown in Figure 3, for both resolutions as well as for three

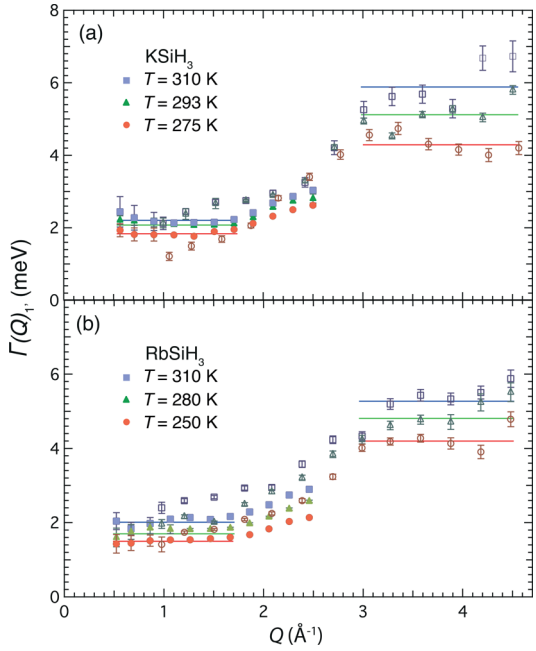

Figure 3. $\Gamma_{1'}(Q)$ for (a) $KSiH_3$ and (b) $RbSiH_3$, where the data shown with filled and open symbols originate from measurements using 4.8 and 2.5 Å neutrons, respectively. The horizontal lines are least-squares fits within the Q-ranges of 0.56−1.71 and 3.05−4.54 Å^{-1}.

selected temperatures in the disordered α-phase. As can be seen, the $\Gamma_{1'}(Q)$ shows a strong Q-dependence and evolves from a largely Q-independent line width for the lowest Q-values (~0.5−2 Å^{-1}), through a large increase for intermediate Q-values (~2−3 Å^{-1}), back to a largely Q-independent line width for the highest Q-values as investigated here (~3−4.5 Å^{-1}), for both materials. The lines in Figure 3 are constant fits to the data over the two Q-independent ranges and correspond to characteristic relaxation times of approximately 0.7 ps (narrower) and 0.3 ps (broader), respectively. This Q-dependent width behavior is very reasonable for jump-diffusion mechanisms involving multiple jump locations and thus indicates a more complicated dynamical process.[29] The width behavior of the single quasielastic component, $L_{1'}(Q, \omega)$, suggested that it should actually be further separated into two Lorentzian components [$L_1(Q, \omega)$ and $L_2(Q, \omega)$], with widths according to the Q-averaged values shown in Figure 3. Thus, the spectra were ultimately fit with a function comprised of one elastic component, appearing as a delta function, and three Lorentzian functions, of which two, $L_1(Q, \omega)$ and $L_2(Q, \omega)$, describe the quasielastic scattering, and the third one, $L_3(Q, \omega)$, represents the background, i.e.

$$S_{inc}(Q, \omega) = A_0(Q)\delta(\omega) + A_1(Q)L_1(Q, \omega) + A_2(Q)L_2(Q, \omega) + A_3(Q)L_3(Q, \omega) \quad (5)$$

DOI: 10.1021/acs.jpcc.6b00363
J. Phys. Chem. C 2016, 120, 6369−6376

In Figure 4 is shown, as an example, the fit to the experimental data for T = 310 K and Q = 2.1 Å^{-1}, as measured

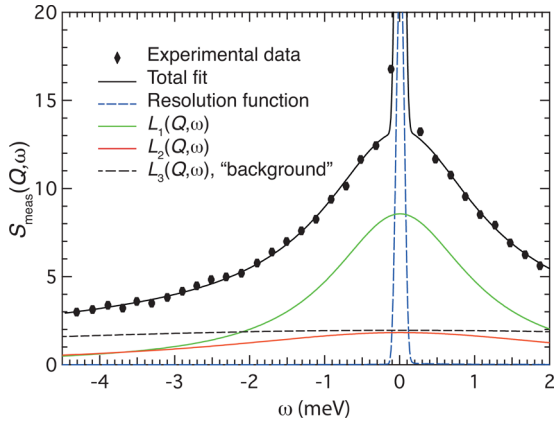

Figure 4. $S_{meas}(Q, \omega)$ of $KSiH_3$ at T = 310 K and Q = 2.1 Å^{-1}, as measured with 4.8 Å neutrons. The solid lines are fits to the experimental data according to eq 5.

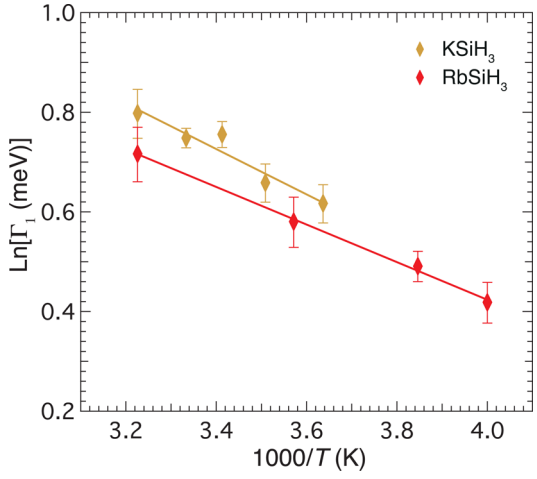

Figure 5. Arrhenius plot of $\Gamma_1(Q)$ for $KSiH_3$ and $RbSiH_3$. The fits correspond to activation energies of 39(1) meV for $KSiH_3$ and 33(1) meV for $RbSiH_3$.

using 4.8 Å neutrons. Figure 5 shows an Arrhenius plot of the quasielastic width of the narrowest component, $\Gamma_1(Q)$, since this represents the fundamental jump correlation frequency and is also the one least affected by the background related to inelastic scattering contributions. The $\Gamma_1(Q)$ follows an Arrhenius dependence with activation energies of 39(1) meV for $KSiH_3$ and 33(1) meV for $RbSiH_3$. This is comparable to the activation energies for BH_4^- motions in $LiBH_4$ (68 meV) and 1:1 $LiBH_4$–LiI solid solution (36 meV), respectively.[11,24] For comparison, activation energies of BH_4^- motions in the heavier alkali borohydrides $NaBH_4$ and KBH_4 are in the range 100–150 meV and thus considerably higher.[23,24]

4.2. Experimental Determination of the EISF and Model Calculations. Since the QENS spectra are measured as a function of Q, the geometry of the observed localized motion(s) can be obtained from the Q-dependence of the elastic part of the scattering function $A_0(Q)$ [eq 5], which is commonly called the elastic incoherent structure factor (EISF). The EISF provides a measure of the time-averaged spatial distribution of hydrogens and hence gives information about the geometry of the reorientational motions of SiH_3^- ions. The EISF is determined experimentally as the ratio of the elastic (incoherent) scattering intensity to the total (incoherent) scattering intensity, plotted as a function of Q. The total incoherent scattering intensity is the sum of the intensities of the elastic and quasielastic scattering and follows the assumption that the quasielastic and vibrational motions are separable, i.e., they occur on different time-scales. However, we have seen that in our case this assumption is not entirely valid, because there is some overlap between inelastic and quasielastic scattering as reflected by the broader Lorentzian function, $L_3(Q, \omega)$. Therefore, the EISF has been derived by neglecting the broadest Lorentzian, i.e.

$$\mathrm{EISF} = \frac{A_0(\mathrm{Q})}{A_0(\mathrm{Q}) + A_1(\mathrm{Q}) + A_2(\mathrm{Q})} \quad (6)$$

The EISF is unity at Q = 0 and falls to a minimum at a Q-value that, importantly, relates to the spatial geometry of the dynamics. For instance, for a jump motion between three equivalent sites, the EISF is an oscillatory function of Q that approaches 1/3 at large values of Q, whereas a jump motion between four equivalent sites yields a different oscillatory EISF function that approaches 1/4 at large values of Q. Therefore, by comparing the experimental EISF with geometrically feasible models, the geometry of motion can often be revealed. The EISFs for these models are, however, often very similar to one another at small Q-values. Therefore, higher-Q data are often needed to distinguish between likely models. This requires using higher-energy (shorter-wavelength) neutrons, but necessarily results in poorer energy resolution, which is a largely unavoidable characteristic of neutron spectrometers. Here, we measure QENS spectra up to a Q-value of 4.48 Å^{-1}, which is sufficiently large in order to allow for a distinction between relevant models.

As the dynamics of most molecular solids primarily involve rotational jumps of the molecules about their high-symmetry axes, attempts to fit the data were first naturally made on the basis of models describing rotational diffusion of the SiH_3^- ion about its principal axis (and neglecting the various possible orientations in the unit cell), cf. Figure 1(b). Note that compared to C_{3v} SiH_3^-, the rotational behavior of T_d BH_4^- ions in cubic ABH_4 phases is much more transparent. These are 90° reorientations around the three C_2 axes (resulting in a cubic H environment around the B atoms) and 120° rotations around the four C_3 axes.

For SiH_3^-, first attempts were based on models describing rotational motion between the three equivalent sites around the C_3 axis, as well as free rotation about this axis. A comparison with the experimentally determined EISF (Figure 6) suggests that free rotation about the C_3 axis is a better description than discrete 3-fold jump reorientations, but none of these fits are satisfactory. This result might have been expected, however, because the quasi-spherical arrangement with 24 H atom positions around each Si atom means that we have to consider reorientation models that do not necessarily preserve a particular orientation of the SiH_3^- ions in the NaCl-type crystal structure. For this reason, we also tried to fit the data using a model describing jump diffusion on the surface of a sphere, with 24 different jump locations. In addition, we considered the limiting case of isotropic rotational diffusion,

DOI: 10.1021/acs.jpcc.6b00363
J. Phys. Chem. C 2016, 120, 6369–6376

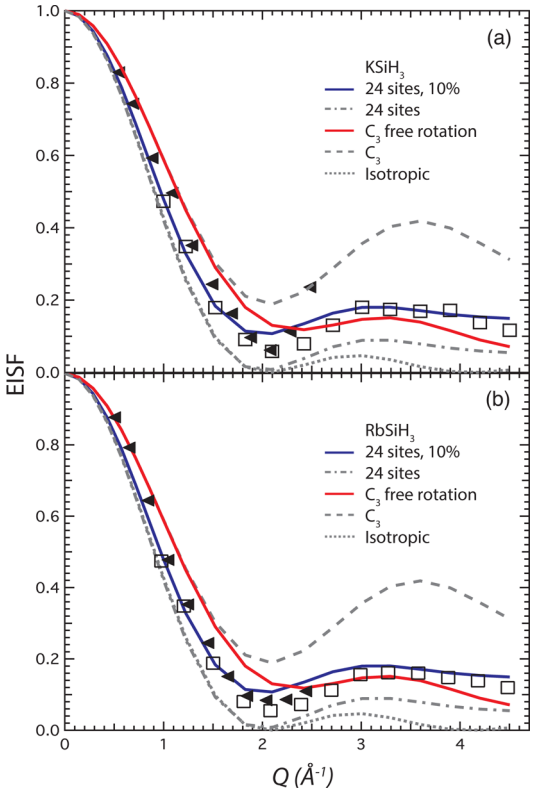

Figure 6. Experimental and modeled EISFs for (a) $KSiH_3$ and (b) $RbSiH_3$ at 310 K. Data obtained using 2.5 Å neutrons are represented by open squares, whereas data obtained using 4.8 Å neutrons are represented by filled triangles. The error bars are within the size of the symbols. The constant of 0.1 (10%) as added to the 24-site model (blue) accounts for QENS intensity in the subtracted background and/or to the scattering from H hidden in the elastic peak.

meaning that the molecule is free to reorient in any direction with small jump distances. Nevertheless, none of these models, which are mathematically defined in the SI, fit well to the data. However, a satisfactory, and physically sound, fit was obtained using the 24-site model plus a constant of 0.1, i.e

$$\mathrm{EISF}_{24\ \mathrm{sites,10\%\ immobile\ H}} = 0.9 \times \mathrm{EISF}_{24\ \mathrm{sites}} + 0.1 \quad (7)$$

where

$$\mathrm{EISF}_{24\ \mathrm{sites}} = \frac{1}{24}[1 + j_0(Qd_1) + j_0(Qd_2) + \ldots j_0(Qd_{23})] \quad (8)$$

and the 23 jump distances (d_1, d_2,..., d_{23}) correspond to the 24 different H locations of α-$ASiH_3$, which have been determined on the basis of neutron diffraction data and are shown in the SI. The constant of 0.1 (10%) reflects scattering of H atoms that do not contribute to the observed dynamics, perhaps relating to the presence of lingering low-temperature (β) phase fractions, and/or to minor amounts of AH impurity phases,[21] cf. Figure 6. Moreover, there may be some quasielastic scattering intensity that we are ignoring in the very broad inelastic background component, which will tend to lower the experimentally observed EISF curve even closer to that for the 24-site model. In fact, the latter prospect is consistent with the slight increase in the quasielastic intensity that we observe when the sample is cooled from 310 to 275 K for $KSiH_3$ and from 310 to 250 K for $RbSiH_3$, cf. Figure 2. This behavior is likely due to the transferring of some uncounted quasielastic intensity from the very broad Lorentzian background to the intensities of the quasielastic components. Such missing quasielastic intensity would become more visible with decreasing temperature toward the phase transition as it comes into the experimentally accessible time-scale of the instrument.

The small differences between the experimental and modeled EISF at the lowest Q-values, for all models as considered here, are most likely related to well-known artifacts of multiple scattering, which are mainly noticeable at small angles. Figure 7

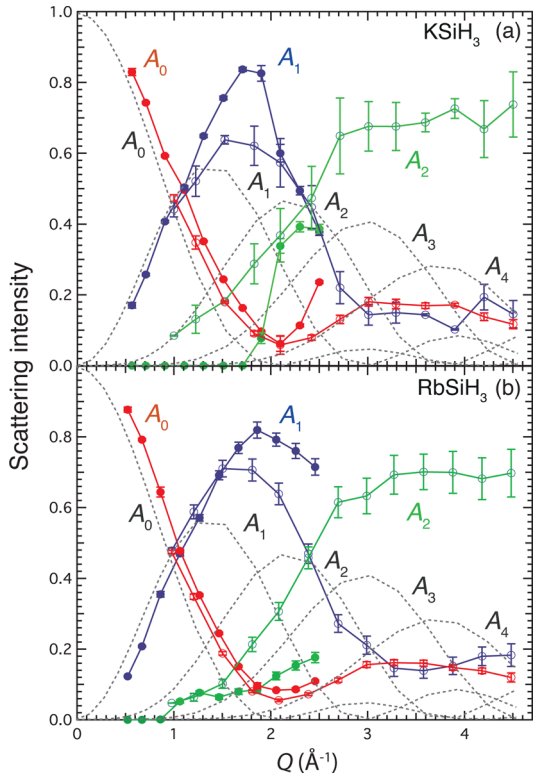

Figure 7. Observed normalized intensities of the elastic line (red), narrower Lorentzian (blue), and wider Lorentzian (green), as a function of Q for the fitted functions at 310 K, for (a) $KSiH_3$ and (b) $RbSiH_3$, respectively. Data shown with filled and open symbols originate from measurements using 4.8 and 2.5 Å neutrons, respectively. Also the theoretical intensities for an isotropic rotational diffusion model (as dashed gray lines), are included in the figure.

shows the relative intensities of the elastic line (EISF) together with the area of the two Lorentzian functions [$L_1(Q, \omega)$ and $L_2(Q, \omega)$] as a function of Q at 310 K for both materials. Also included in the figure are the intensities of the elastic and first three Lorentzian functions for an isotropic rotational diffusion model, which is a good approximation of the 24-site model, particularly below a Q-value of ~2.5 $Å^{-1}$ (see Figure 6). There is a good agreement with the experimental and theoretical data, but even more noticeable is the fact that the narrower Lorentzian, $L_1(Q, \omega)$, should most likely be divided further into two additional Lorentzians at Q values above around 1 $Å^{-1}$. Experimentally, however, the statistics of the data limit the ability to distinguish quasielastic features with similar line widths, especially if one quasielastic feature dominates the spectrum at a given Q. This is the reason that we only use two Lorentzian functions to fit the quasielastic scattering (+ a third Lorentzian, which describes the "background"), but theoret-

DOI: 10.1021/acs.jpcc.6b00363
J. Phys. Chem. C 2016, 120, 6369−6376

ically a sequence of different Lorentzian functions, associated with the 24-site model, should be used.

We stress that the observed EISFs at high Q values combined with the known disordered α-phase structures suggest that we are dealing with H atoms more localized around the eight corners of a cube defined by the various possible SiH_3^- C_3 symmetry axes rather than full H orientational disorder over the surface of a sphere (isotropic rotational diffusion). It is possible that the extra 10% elastic scattering intensity required to reconcile the minor discrepancies between model and experimental EISFs may be an indication that the 3-dimensionality of the reorientations are not yet fully realized (with the resolution used), i.e., the reorientations around any particular 3-fold axis are very rapid but the changes among the eight possible axes are much slower and not yet fully separable from the elastic peak. Such an intermediate type EISF behavior has been seen when there is a change from lower dimensionality to higher dimensionality, as exemplified for BH_4^- reorientations in orthorhombic $LiBH_4$ and in hexagonal $LiBH_4$–LiI solid solutions.[9,10]

By bringing together the results from the QENS analysis, we can now understand several new features related to both the structure and dynamics of $ASiH_3$ (A = K and Rb). A key result is the observation of an onset of SiH_3^- rotational dynamics at the order–disorder phase transition with increasing temperature. The dynamics is manifested by reorientational motion of the SiH_3^- anions, characterized by a relaxation time of slightly less than one picosecond and with a quite weak temperature dependence, with no large difference between the two materials. Instead, the strongest effect of the type of alkali ion is seen on the phase transition temperature, at about 300 K for $KSiH_3$ and at about 285 K for $RbSiH_3$ and also seen in the small difference in activation energies (39 and 33 meV, respectively). This difference may be attributed to the difference in atomic radii between 6-fold coordinated K (152 pm) and Rb (166 pm),[30,31] since the slightly more spacious structure of $RbSiH_3$ may favor the earlier onset of dynamics.

5. CONCLUSIONS

We have investigated the dynamical behavior of hydrogen atoms in the two alkali silanides $ASiH_3$ (A = K and Rb) using QENS, both below and above the order–disorder (β–α) phase transition occurring at around 275–300 K. The results show that the phase transition leads to dynamical changes corresponding to the onset of rapid reorientational motions of the pyramidal SiH_3^- ions. The SiH_3^- dynamics is adequately modeled by H-jumps between 24 different jump locations distributed radially around the Si atom, which is in agreement with the structure of α-$ASiH_3$. The average relaxation time between successive jumps is of the order of subpicoseconds and exhibits a weak temperature dependence with a small difference in activation energy between the two materials, 39(1) meV for $KSiH_3$ and 33(1) meV for $RbSiH_3$. Besides being of considerable fundamental interest, our better understanding of the nature of the SiH_3^- orientational mobility in the disordered phases of $KSiH_3$ and $RbSiH_3$, explains the high entropy observed in the α-phase resulting in the low entropy variation for hydrogen absorption/desorption and hence the origin of these materials' favorable hydrogen storage properties.

■ ASSOCIATED CONTENT

Supporting Information

The Supporting Information is available free of charge on the ACS Publications website at DOI: 10.1021/acs.jpcc.6b00363.

Mathematical description of the EISFs and the specific jump distances, as well as the goodness of the fits of the neutron data (PDF)

■ AUTHOR INFORMATION

Corresponding Author

*Fax: +46 31 772 2090. Tel: +46 31 772 8038. E-mail: maths.karlsson@chalmers.se.

Notes

The authors declare no competing financial interest.

■ ACKNOWLEDGMENTS

This research was funded by the Swedish Foundation for Strategic Research (Grant No. ICA10-0001), the Swedish Research Council (Grant No. 2010-3519), and the U.S. DOE EERE (Grant No. DE-EE0002978). A travel grant by the Chalmers Area of Advance in Materials Science is also gratefully acknowledged. The NIST Center for Neutron Research is thanked for access to neutron beam facilities. This work utilized facilities supported in part by the NSF under Agreement No. DMR-0944772.

■ REFERENCES

(1) Schlapbach, L.; Züttel, A. Hydrogen-Storage Materials for Mobile Applications. *Nature* **2001**, *414*, 353–358.
(2) Eberle, U.; Felderhoff, M.; Schüth, F. Chemical and Physical Solutions for Hydrogen Storage. *Angew. Chem., Int. Ed.* **2009**, *48*, 6608–6630.
(3) Chotard, J.-N.; Tang, W. S.; Raybaud, P.; Janot, R. Potassium Silanide ($KSiH_3$): A Reversible Hydrogen Storage Material. *Chem. - Eur. J.* **2011**, *17*, 12302–12309.
(4) Tang, W.; Chotard, J.; Raybaud, P.; Janot, R. Enthalpy-Entropy Compensation Effect in Hydrogen Storage Materials: Striking Example of Alkali Silanides $MSiH_3$ (M = K, Rb, Cs). *J. Phys. Chem. C* **2014**, *118*, 3409–3419.
(5) Chen, P.; Xiong, Z.; Luo, J.; Lin, J.; Tan, K. L. Interaction of Hydrogen with Metal Nitrides and Imides. *Nature* **2002**, *420*, 302–304.
(6) Chen, P.; Xiong, Z.; Luo, J.; Lin, J.; Tan, K. L. Interaction between Lithium Amide and Lithium Hydride. *J. Phys. Chem. B* **2003**, *107*, 10967–10970.
(7) Züttel, A.; Rentsch, S.; Fischer, P.; Wenger, P.; Sudan, P.; Mauron, P.; Emmenegger, C. Hydrogen Storage Properties of $LiBH_4$. *J. Alloys Compd.* **2003**, *356–357*, 515–520.
(8) Züttel, A.; Borgschulte, A.; Orimo, S. Tetrahydroborates as New Hydrogen Storage Materials. *Scr. Mater.* **2007**, *56*, 823–828.
(9) Verdal, N.; Hartman, M. R.; Jenkins, T.; DeVries, D.; Rush, J. J.; Udovic, T. J. Reorientational Dynamics of $NaBH_4$ and KBH_4. *J. Phys. Chem. C* **2010**, *114*, 10027–10033.
(10) Verdal, N.; Udovic, T. J.; Rush, J. J. The Nature of BH_4^- Reorientations in Hexagonal $LiBH_4$. *J. Phys. Chem. C* **2012**, *116*, 1614–1618.
(11) Verdal, N.; Udovic, T. J.; Rush, J. J.; Wu, H.; Skripov, A. V. Evolution of the Reorientational Motions of the Tetrahydroborate Anions in Hexagonal $LiBH_4$-LiI Solid Solution by High-Q Quasielastic Neutron Scattering. *J. Phys. Chem. C* **2013**, *117*, 12010–12018.
(12) Verdal, N.; Udovic, T. J.; Rush, J. J.; Liu, X.; Majzoub, E. H.; Vajo, J. J.; Gross, A. F. Dynamical Perturbations of Tetrahydroborate Anions in $LiBH_4$ due to Nanoconfinement in Controlled-Pore Carbon Scaffold. *J. Phys. Chem. C* **2013**, *117*, 17983–17995.

DOI: 10.1021/acs.jpcc.6b00363
J. Phys. Chem. C 2016, 120, 6369–6376

(13) Bogdanovic, B.; Schwickardi, M. Ti-doped Alkali Metal Aluminium Hydrides as Potential Novel Reversible Hydrogen Storage Materials. *J. Alloys Compd.* **1997**, *253*−*254*, 1−9.
(14) Bogdanovic, B.; Brand, R. A.; Marjanovic, A.; Schwickardi, M.; Tolle, J. Metal-Doped Sodium Aluminium Hydrides as Potential New Hydrogen Storage Materials. *J. Alloys Compd.* **2000**, *302*, 36−58.
(15) Xiong, Z.; Yong, C. K.; Wu, G.; Chen, P.; Shaw, W.; Karkamkar, A.; Autrey, T.; Jones, M. O.; Johnson, S. R.; Edwards, P. P.; et al. High-Capacity Hydrogen Storage in Lithium and Sodium Amidoboranes. *Nat. Mater.* **2008**, *7*, 138−141.
(16) Verdal, N.; Udovic, T. J.; Rush, J. J.; Stavila, V.; Wu, H.; Zhou, W.; Jenkins, T. Low-Temperature Tunneling and Rotational Dynamics of the Ammonium Cations in $(NH_4)_2B_{12}H_{12}$. *J. Chem. Phys.* **2011**, *135*, 094501−8.
(17) Wu, H.; Zhou, W.; Pinkerton, F. E.; Udovic, T. J.; Yildirim, T.; Rush, J. J. Metal Hydrazinoborane $LiN_2H_3BH_3$ and $LiN_2H_3BH_3{\cdot}2N_2H_4BH_3$: Crystal Structures and High-Extent Dehydrogenation. *Energy Environ. Sci.* **2012**, *5*, 7531−7535.
(18) Ring, M. A.; Ritter, D. M. Preparation and Reactions of Potassium Silyl. *J. Am. Chem. Soc.* **1961**, *83*, 802−805.
(19) Weiss, E.; Hencken, G.; Kuhr, H. Kristallstrukturen und Kernmagnetische Breitlinienresonanz der Alkalisilyle SiH_3M (M = K, Rb, Cs). *Chem. Ber.* **1970**, *103*, 2868−2872.
(20) Mundt, O.; Becker, G.; Hartmann, H.-M.; Schwarz, W. Z. Darstellung und Struktur des beta-Kaliumsilanids. *Z. Anorg. Allg. Chem.* **1989**, *572*, 75−88.
(21) Kranak, V. F.; Lin, Y.-C.; Karlsson, M.; Mink, J.; Norberg, S. T.; Häussermann, U. Structural and Vibrational Properties of Silyl (SiH_3^-) Anions in $KSiH_3$ and $RbSiH_3$: New Insight into Si-H Interactions. *Inorg. Chem.* **2015**, *54*, 2300−2309.
(22) Karlsson, M. Proton Dynamics in Oxides: Insight into the Mechanics of Proton Conduction from Quasielastic Neutron Scattering. *Phys. Chem. Chem. Phys.* **2015**, *17*, 26−38.
(23) Remhof, A.; Lodziana, Z.; Buchter, F.; Martelli, P.; Pendolino, F.; Friedrichs, O.; Züttel, A. Embs. Rotational Diffusion in $NaBH_4$. *J. Phys. Chem. C* **2009**, *113*, 16834−16837.
(24) Remhof, A.; Lodziana, Z.; Martelli, P.; Friedrichs, O.; Züttel, A.; Skripov, V. A.; Embs, J. P.; Strässle, T. Rotational Motion of BH_4 Units in MBH_4 (M = Li, Na, K) from Quasielastic Neutron Scattering and Density Functional Calculations. *Phys. Rev. B: Condens. Matter Mater. Phys.* **2010**, *81*, 214304:1−9.
(25) Jimura, K.; Hayashi, S. Reorientational Motion of BH_4 Ions in Alkali Borohydrides MBH_4 (M = Li, Na, K) as Studied by Solid-State NMR. *J. Phys. Chem. C* **2012**, *116*, 4883−4891.
(26) The mention of all commercial suppliers in this paper is for clarity and does not imply the recommendation or endorsement of these suppliers by NIST.
(27) Copley, J. R. D.; Cook, J. C. The Disk Chopper Spectrometer at NIST: A New Instrument for Quasielastic Neutron Scattering Studies. *Chem. Phys.* **2003**, *292*, 477−485.
(28) Azuah, R.; Kneller, L.; Qiu, Y.; Tregenna-Piggott, P. L. W.; Brown, C.; Copley, J.; Dimeo, R. DAVE: A Comprehensive Software Suite for the Reduction, Visualization, and Analysis of Low Energy Neutron Spectroscopic Data. *J. Res. Natl. Inst. Stand. Technol.* **2009**, *114*, 341−358.
(29) Bée, M. *Quasielastic Neutron Scattering, Principles and Applications in Solid State Chemistry, Biology and Materials Science*; Adam Hilger: Bristol, U.K., 1988.
(30) Renaudin, G.; Gomes, S.; Hagemann, H.; Keller, L.; Yvon, K. Structural and Spectroscopic Studies on the Alkali Borohydrides MBH_4 (M = Na, K, Rb, Cs). *J. Alloys Compd.* **2004**, *375*, 98−106.
(31) Shannon, R. D. Revised Effective Ionic Radii and Systematic Studies of Interatomic Distances in Halide and Chalcogenides. *Acta Crystallogr., Sect. A: Cryst. Phys., Diffr., Theor. Gen. Crystallogr.* **1976**, *32*, 751−767.

DOI: 10.1021/acs.jpcc.6b00363
J. Phys. Chem. C 2016, 120, 6369−6376

Supporting Information for:

Dynamics of Pyramidal SiH_3^- Ions in $ASiH_3$ (A = K and Rb) Investigated with Quasielastic Neutron Scattering

Carin Österberg[1], Henrik Fahlquist[2], Ulrich Häussermann[2], Craig M. Brown[3], Terrence J. Udovic[3], Maths Karlsson[1,*]

[1]Department of Applied Physics, Chalmers University of Technology, SE-412 96 Göteborg, Sweden. Fax: +46 31 772 2090; Tel: +46 31 772 8038; E-mail: maths.karlsson@chalmers.se (Maths Karlsson). [2]Department of Materials and Environmental Chemistry, Stockholm University, SE-10691 Stockholm, Sweden. [3]NIST Center for Neutron Research, National Institute of Standards and Technology, 100 Bureau Drive, Gaithersburg, Maryland 20899-6102, United States.

1 EISF models

A general expression for the EISF (A_0) can be generated for N number of equivalent sites according to

$$A_0(Q) = \frac{1}{N}\sum_{n=1}^{N} j_0(Qr_n), \quad (1)$$

where j_0 is the zeroth-order spherical Bessel function ($j_0 = \sin(x)/(x)$).[S1] In our case, the experimental data was fit to models characterized by jumps between three equivalent sites (C_3 axis rotations), as well as free rotations around this axis (C_3 free rot.). We also fit the data using a model describing jump diffusion on the surface of a sphere with 24 different jump locations, corresponding to the H atom position in α-$ASiH_3$ (see Fig. 1), as well as the limiting case of isotropic rotational diffusion. The mathematical expressions for these EISF models are shown below. Their derivation can be found elsewhere.[S1–S3]

(1) C_3 axis rotations:

$$\mathrm{EISF}_{C_3} = \frac{1}{3}[1 + 2j_0(\sqrt{2}r_1Q)]. \quad (2)$$

(2) Free rotational diffusion around the C_3 axis:

$$\mathrm{EISF}_{\text{free rot.}} = \frac{1}{N}\sum_{n=1}^{N} j_0[2Qr\sin(\frac{n\pi}{N})], \quad (3)$$

where N is large ($\geq$50) and the rotational diffusion may be considered as free diffusion around a circle with radius r.

(3) Isotropic rotational diffusion on a sphere:

$$\mathrm{EISF}_{\text{iso}} = j_0^2(Qr). \quad (4)$$

In this case, the pyramidal SiH_3^- molecule may be seen to rotate freely in all directions with jump distances corresponding to the surface of a sphere with radius r.

(4) Rotational diffusion on a sphere with 24 different jump locations:

$$\mathrm{EISF}_{24\text{ sites}} = \frac{1}{24}[1 + j_0(Qd_1) + j_0(Qd_2) + \ldots j_0(Qd_{23})], \quad (5)$$

where the 23 jump distances (d_1, d_2,..., d_{23}) correspond to the 24 different H locations of α-$ASiH_3$, which have been determined on the basis of neutron diffraction data.[S4] Fig. S1 shows these jump distances as determined from a central H atom (labelled as x in the figure). The jump distances are also presented in Table S1. In order to account for the 10% of immobile H atoms, as described in the article, the following model, which fits adequately to the data, was constructed:

$$\mathrm{EISF}_{24\text{ sites,10\% immobile H}} = 0.9 \times \mathrm{EISF}_{24\text{ sites}} + 0.1. \quad (6)$$

Table S1 H jump distances in SiH_3^-, with respect to a central H atom (see text and Fig. S1).

Number of distances	Distances (Å)
2	0.6028
1	1.1271
4	1.6108
2	1.9797
2	2.0694
2	2.1968
2	2.2780
4	2.5522
1	2.7996
2	2.9738
1	3.0180

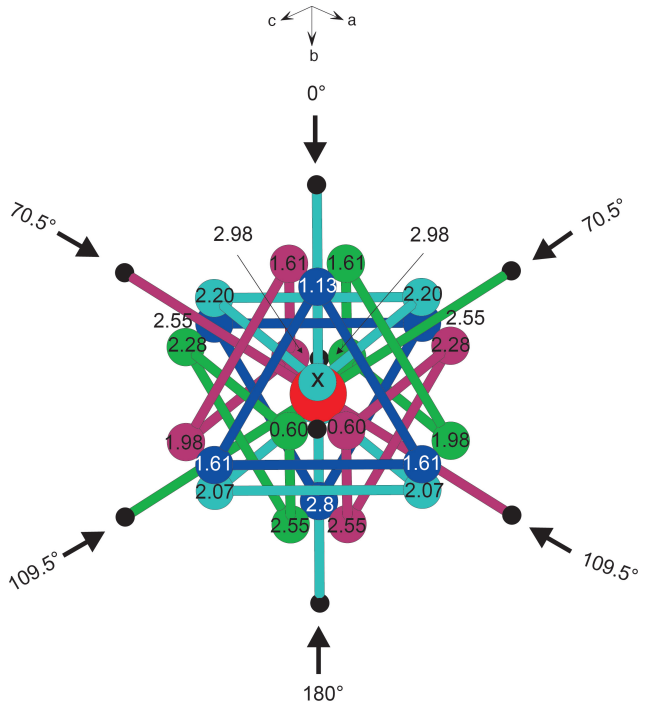

Fig. S1 Schematic depiction of the 24 H-atom environments in ASiH$_3$, as a consequence of aligning pyramidal SiH_3^- ions (with respect to their C_3 axis) randomly along the four body diagonals of the cubic unit cell (see also Fig. 1). Hence, there will be three principally different types of reorientational motions of the C_3 axis, corresponding to the different angles between the four body diagonals of a cube: 0→70.5° (3 possibilities), 0→109.5° (3 possibilities), and 0→180° (one possibility). The 23 jump distances (in units of Å) from a central H atom (labelled as x) are indicated.

2 Quality of the fitting to the QENS spectra

The QENS spectra were fit by least-squares fitting. As an example, the average values of the goodness of the fits (χ^2) at 310 K are 2.42 (4.8 Å) and 1.93 (2.5 Å) for KSiH$_3$, and 2.14 (4.8 Å) and 3.49 (2.5 Å) for RbSiH$_3$, where the numbers within parentheses refer to the neutron wavelength.

References

S1 Bée, M. *Quasielastic Neutron Scattering, Principles and Applications in Solid State Chemistry, Biology and Materials Science*: Adam Hilger: Bristol, UK, 1988.

S2 Yildirim, T.; Gehring, P. M.; Neumann, D. A.; Eaton, P. E.; and Emrick, T. Neutron-Scattering Investigation of Molecular Reorientations in Solid Cubane. *Phys. Rev. B* **1999**, *60*, 314–321

S3 Dianoux, A. J.; Volino F.; Hervet, H. Incoherent Scattering Law for Neutron Quasi-Elastic Scattering in Liquid Crystals. *Mol. Phys.* **1975**, *30*, 1181–1194

S4 Kranak, V. F.; Lin, Y.-C.; Karlsson, M.; Mink, J.; Norberg, S. T.; Häussermann, U. Structural and Vibrational Properties of Silyl (SiH_3^-) Anions in KSiH$_3$ and RbSiH$_3$: New Insight into Si-H Interactions. *Inorg. Chem.* **2015**, *54*, 2300–2309